Proceedings of The Canadian Society for Mechanical Engineering International Congress 2016
CSME International Congress 2016
June 26-29, 2016, Kelowna, BC, Canada

EXPERIMENTAL CHARACTERIZATION OF BRUSHLESS DC MOTORS AND PROPELLERS FOR FLIGHT APPLICATION

Dominic Muzar Eric Lanteigne

***Abstract*—** Although there exist a number of accurate UAV thruster models, these models require precise measurements of several motor and propeller characteristics. This paper presents simple motor and propeller models based solely on data provided by manufacturers. The theoretical performance predictions for the motors and propellers are computed and then compared to experimental results obtained in static thrust tests. The objective is to confirm the accuracy of the models and facilitate the selection of appropriate brushless DC motor and propeller combinations for flight applications.

Keywords- brushless DC motor; propeller; model; unmanned aerial vehicle

I. INTRODUCTION

Electric motors offer a compact, power dense, reliable power plant making them ideal for use in small aeronautic vehicles like drones and UAVs. In particular, induction, brushed DC, and brushless DC motors are well suited to this application [1]. Among these, the brushless DC (BLDC) motor stands out on account of its high power density, efficiency, and reliability. The availability of small, inexpensive power electronics have made BLDC motors more cost-competitive and increasingly popular for UAV applications such as in [1, 2, 3, 4, 5, 6].

BLDC motors typically have permanent magnets integrated to the rotor while the stator houses the windings. They function similarly to synchronous motors, that is by sequentially energizing the stator windings causing the rotor to turn due to alignment torque. The BLDC motor uses an Electronic Speed Control (ESC) circuit, to perform the commutation. In addition to the stator, rotor, and ESC, BLDC motors can include position sensors such as optical encoders or Hall effect sensors to monitor the position of the rotor and perform the commutation more effectively. These sensors can significantly impact motor efficiency, reliability, and performance [7]; and as a result, several, typically larger, BLDC motors use such sensors.

The family of BLDC motors subdivides into two distinctive categories: axial flux and radial flux motors. Radial flux motors are more common, being studied and used in a larger number of applications. However, some research suggests that the axial flux design may yield a smaller, lighter, and more efficient motor [8, 9]. Although promising, current research on axial flux motors limits their use in hand-size drones or UAVs (i.e. in the range of 50 W). Furthermore, axial flux motors of this power range are not readily available commercially-off-the-shelf (COTS).

Among radial flux motors, there are two subcategories: inrunner and outrunner motors. The former has the stator surrounding the rotor while in the latter, the rotor surrounds the stator. The advantage of outrunner BLDC motors is that they have lower speeds and higher torque making them useful for direct-drive applications as in [2, 5, 10, 11]. Here, the rotor shaft is directly fixed to a propeller without any gearing thereby reducing the weight and complexity of the vehicle, eliminating transmission losses, and reducing costs.

The design of a drone or UAV entails proper selection of a motor and propeller combination. In order to perform this selection, it is important to quantify the speed-voltage and torque-current characteristics of the motor as well as the speed-torque-thrust characteristics of propellers. Since motors and propellers have narrow bands of high efficiency operating conditions, a proper selection identifies a propeller which will produce enough thrust to maintain a steady flying altitude while turning at a speed which is optimal for the motor-propeller combination's performance.

Manufacturers of COTS BLDC motors rarely include test data identifying the motors' operating characteristics. Instead, general motor characteristics are given such as the speed constant, the winding resistance, and the current at no-load. Similarly, manufacturers of COTS propellers for use in small aircrafts provide very little information about the propeller's performance or geometry. The only data consistently provided are the propeller's diameter and pitch (usually quoted at 75% of the radius in the case of twisted blades).

Although accurate models are important when developing UAV control systems, it can be useful to quickly approximate motor and propeller performance without the hassle of measuring and testing the products in a laboratory setting. Therefore,

This work was supported by the NSERC Discovery Grant RGPIN-2014-04501.

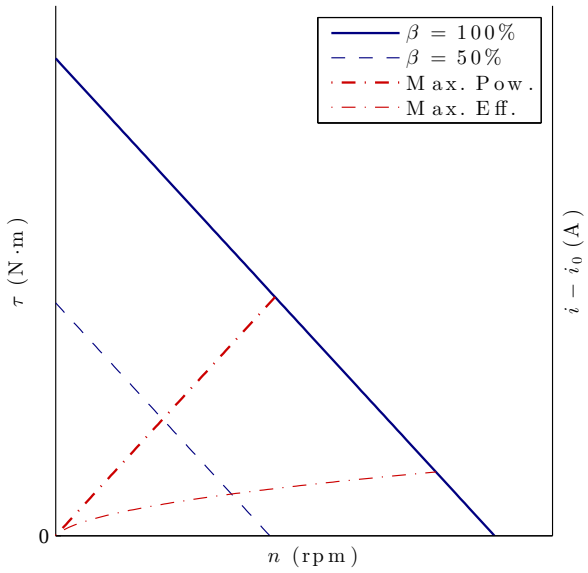

Figure 1. Qualitative Speed-Torque-Current Characteristics of a Brushless DC Motor at a Constant Driving Voltage

this paper aims to validate simple models with the purpose of canvasing the market for an appropriate BLDC motor and propeller combination.

II. Modelling

A. *Modelling BLDC Motors*

Permanent magnet motors are characterized by linear relations between the speed, n, and electro-motive force (EMF) as well as between the torque, τ, and current [12]. The relation is qualitatively shown by the solid line in Figure 1 for a permanent magnet motor with a constant driving voltage. Here, the legend identifies the line as $\beta = 100\%$. The variable β represents the PWM duty cycle of the ESC: when $\beta = 100\%$ the motor is at full speed, when $\beta = 0\%$ the motor is stopped. Referring to Figure 1, first note that as the torque increases, so does the current. Second, note that as torque increases, speed decreases despite a constant driving voltage.

The relation between torque and speed is explained by a motor circuit analysis. Consider the simplified motor and ESC circuit shown in Figure 2. Since at any moment only two of the three windings are energized, the supply voltage, V_s, the back EMF produced by rotation, E_b, the current passing through the windings, i, and the winding resistance, R_m, are related by Kirchoff's voltage law: $V_s = E_b + iR_m$. It follows that for a constant supply voltage, the back EMF and current are inversely proportional: $E_b \propto \frac{1}{i}$. Given that the torque is proportional only to the current, a constant load will draw a fixed amount of current and the remaining difference will be back EMF ($V_s - iR_m = E_b$). As the load increases, more current is drawn,

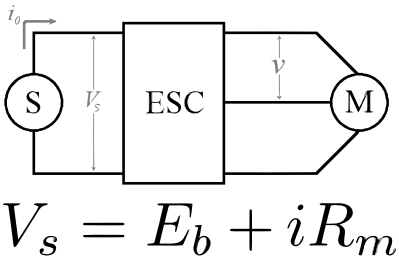

Figure 2. Simplified Circuit Diagram of a Brushless DC Motor with Electronic Speed Control

and the remaining E_b is smaller. Since E_b is proportional to speed, the motor then slows.

The fact that motor speed is dependent on load can make it a difficult parameter to control. ESCs are used to overcome this problem and allow independent control of speed through pulse width modulation (PWM). PWM is the rapid connection/disconnection of the power supply to mimic the effect of a lower supply voltage and shift the speed-torque curve downwards, or to the left. The effect of the ESC is shown by the dashed line $\beta = 50\%$ in Figure 1. In this example, connecting the motor 50% of the time will result in a speed-torque-current curve that resembles a power supply 50% smaller than the one actually being used. The ESC's effect may be described by the following relation:

$$v = \beta V_s \tag{1}$$

Where v is the equivalent driving voltage (V) as seen by the motor and V_s is the power supply voltage (V) as seen by the ESC.

The linear relations between the speed and EMF as well as between the torque and current are provided in (2) and (3). Their proportionality constants are respectively called the motor's speed constant, K_v (rpm/V), and torque constant, K_t (N·m/A). The relationship is described as:

$$n = K_v E_b = K_v(v - iR_m) \tag{2}$$

$$\tau = K_t(i - i_0) \tag{3}$$

Where n is the motor's shaft speed (rpm), τ is its output torque (N·m), R_m is its winding resistance (Ω), i is its line-peak current (A), and i_0 represents the motor's line-peak current at no-load (A). The current at no-load is subtracted in (3) because this minimum amount of current is required to overcome the motor's intrinsic mechanical resistance; it is present when the motor turns even when τ is zero.

In the case of an ideal brushed DC motor (in which saturation and losses are neglected), the motor speed and torque constants are related through perfect energy conservation by

$P = E_b i = \tau\omega$. It then follows that the motor speed and torque constants are directly proportional to one another:

$$K_t = \frac{60}{2\pi K_v} \tag{4}$$

Hendershot and Miller stress the importance of how motor constants are defined, particularly K_t [12]. The relation in (4) holds true for ideal brushed DC motor as well as ideal squarewave BLDC motors with squarewave drives in which (3) relates torque to the line-peak current. However, the relation must be multiplied by the factor $\sqrt{\frac{3}{2}}$ if (3) is based on the RMS current. Similar conversions, provided in [12], are required for sinewave motors / drives.

Equations (2)-(4) fully define the motor's operating condition (τ and n) as a function of PWM duty cycle and current using only motor data provided by the manufacturer (K_v, i_0, R_m, and V_s). These equations can also be used to identify the driving currents for two operating conditions of particular interest: the points of maximum efficiency and of maximum power. Let the motor's efficiency express the ratio of useful mechanical power output to the electrical power input. Substituting τ and n by the expressions in (2) and (3), the efficiency is given by:

$$\eta = \frac{P_M}{P_E} = \frac{\tau(\frac{2\pi n}{60})}{vi} = \frac{(v - iR_m)(i - i_0)}{vi} \tag{5}$$

Then, taking the derivative of (5) with respect to current yields:

$$\frac{d\eta}{di} = \frac{i_0 v - i^2 R_m}{i^2 v} \tag{6}$$

And setting (6) to zero yields i_e, the driving current at maximum efficiency:

$$i_e = \sqrt{\frac{vi_0}{R_m}} = \sqrt{\frac{\beta V_s i_0}{R_m}} \tag{7}$$

A similar expression can be found for the driving current at peak power by starting with the equation for mechanical power and taking the derivative with respect to driving current.

$$P_M = \tau(\frac{2\pi n}{60}) = (v - iR_m)(i - i_0) \tag{8}$$

$$\frac{dP_M}{di} = v - 2iR_m + i_0 R_m \tag{9}$$

Setting the result to zero then yields i_p, the driving current at peak power:

$$i_p = \frac{v + R_m i_0}{2R_m} = \frac{\beta V s + R_m i_0}{2R_m} \tag{10}$$

The points of maximum efficiency and peak power are functions of the motor's characteristics and β. They may be drawn on the speed-torque plot to identify optimal operating conditions as shown by the the dotted lines in Figure 1. This would be useful if the propeller torque and speed were known and the objective was to source an appropriate BLDC motor.

B. Modelling Propellers

An accurate propeller model should account for the geometric properties such as the blade diameter, blade angle (i.e. pitch), chord length, shape of the airfoil, as well as the way in which each of those parameters varies with respect to radial distance. In addition to the geometric properties, one has to account for the airflow into the propeller, how the flow is modified as it exits the propeller, and how these flows may change as the aircraft travels in any direction.

Since a comprehensive model is complex, it is common to characterize a propeller's performance by non-dimensional coefficients for the thrust, torque, power, efficiency, etc. These coefficients are determined experimentally through static tests or through dynamic tests in a wind tunnel. Although static test results can differ significantly from dynamic tests where large inflow velocities are observed, they are well suited to characterize the performance of propellers for helicopters or quadrotors because these vehicles often hover.

In this paper, only one non-dimensional coefficient is presented. It can be used to obtain values for T, the thrust (N), in the following way:

$$T = C_T \rho \pi d^4 \omega^2 \tag{11}$$

Where C_T is the non-dimensional thrust coefficient, ρ is the density of the fluid (kg/m^3), d is the blade diameter (m), and ω is the propeller's angular velocity (rad/s).

Some researchers have attempted to determine C_T analytically but this requires detailed knowledge of the propellers geometry. Instead, an alternative thrust model is introduced. The relation, proposed by hobbyist Gabriel Staples in 2014, is developed from simple momentum theory and then fit to experimental data. It is of the form:

$$T = \rho\pi \frac{(0.0254 \cdot d)^2}{4} \left(\frac{n}{60} \cdot 0.0254 \cdot p\right)^2 \left(\frac{d}{K_1 \cdot p}\right)^{K_2} \tag{12}$$

Where p is the propeller's pitch (in) and n is its speed (rpm). The constants $K_1 = 3.29546$ and $K_2 = 1.5$ were empirically determined to fit the model with experimental data. Rearranging (12) to resemble (11), a generalized, empirically correlated, thrust coefficient can be obtained as a function of propeller diameter and pitch.

$$C_T = \left(\frac{60}{2\pi}\right)^2 \frac{0.0254^4}{4 \cdot 60^2} K_1^{-K_2} \left(\frac{d}{p}\right)^{K_2 - 2} \tag{13}$$

III. Methodology

In order to validate the models, theoretical predictions are made using the relations from section II. Afterwards, experi-

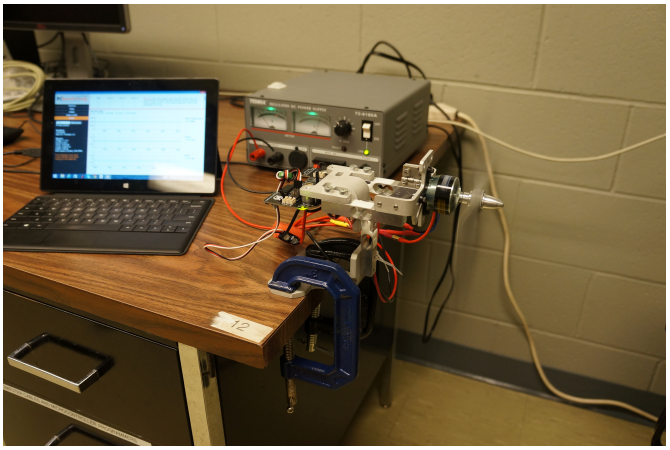

Figure 3. Static Testing of Motor-Propeller Combinations

mental tests are performed on a number of motors and propellers and the results are compared to the theoretical predictions.

A. *Theoretical Predictions*

The theoretical predictions are made for 2 BLDC motors and 22 propellers. The propellers are chosen such that their diameter and pitch fully span and also slightly exceed the range of sizes recommended by the motor's manufacturer.

The theoretical predictions are made with motor characteristics measured experimentally rather than with the manufacturer's data for two reasons: first, experimental values are a better benchmark for validating the motor model since any error is not attributable to differences between the manufacturer's data and the data measured experimentally. Second, the manufacturer provides the motor constants for a supply voltage of 8.0V (roughly 2 Li-Po cells) while the experiments were performed using a supply voltage of 11.1V (the nominal voltage for 3 Li-Po cells) to allow for a broader range of rotational speeds.

The propeller's theoretical predictions are developed using only the propeller's diameter and pitch as provided by the manufacturer.

B. *Experimental Tests*

The experimental data is gathered with the RCBenchmark motor jig used for static testing of motor-propeller combinations. The test setup, shown in Figure 3, is used to measure power source voltage and current, motor mechanical speed (via the measurement of motor electrical speed), motor-propeller static thrust, and torque. Measuring torque allows the motor's performance to be analyzed independently of the propeller's performance.

At first, the motors are tested without a propeller to measure the constants. With the motor running at full speed ($\beta = 100\%$), the current drawn is the no-load current and the motor's speed constant is the ratio of the motor's speed to its supply voltage ($K_v = \frac{n}{V_s}$). The winding resistance is measured by connecting

TABLE I. Manufacturer's & Experimentally Measured Motor Constants at 8.0V

	E-Flite Park 300		**E-Flite Park 450**	
	Manu.	**Meas.**	**Manu.**	**Meas.**
V_S **(V)**	8.0	8.06	8.0	8.06
K_v **(rpm/V)**	1380	1599	1020	1233
$R_m(\Omega)$	0.50	0.48	0.06	0.07
i_0 **(A)**	0.38	0.21	1.10	0.52

two of the motor's leads to the test jig's integral ohmmeter. The resistance is measured when the motor is hot after completing numerous tests to ensure that the measurement reflects an operational state. The motor constants are measured at both 8.0V and 11.1V to enable comparison with the manufacturer's data, and also produce a theoretical model which can be compared to experimental results.

Next, the motors are tested with propellers. The test jig incrementally cycles the PWM duty cycle from $\beta = 0\%$ to $\beta = 100\%$ and back down to $\beta = 0\%$ taking measurements of the voltage, current, speed, thrust, and torque at regular intervals. At each new increment, there is a delay between the time when the duty cycle is increased and the time when data is recorded ensuring that the system has reached a steady-state.

IV. RESULTS

A. *Manufacturer's & Experimentally Measured Motor Constants*

Table I compares the motor characteristics quoted by the manufacturer to the values measured in the laboratory with a supply voltage of 8.0V. The results indicate a significant difference, particularly with regards to K_v and i_0.

The errors associated to the measurement of K_v and i_0 have not been identified. Some sources would dispute that K_v should be measured at the no-load state as well as at multiple points where $\beta = 100\%$ but with varying loads. In this case, a linear regression will more accurately estimate K_v as the quotient of the speed-axis intercept to the source voltage. When used, this method identified a K_v of about 1780 rpm/V and 1210 rpm/V for the E-flite Park 300 and Park 480 respectively. Since the value estimated with no-load is much closer to the manufacturer's value of K_v for the E-flite Park 300, the regression is not used to estimate K_v.

An expected source of error in the measurement of i_0 was the presence of the ESC since it consumes a certain amount of voltage and current meaning the values seen by the motor are lower than the values recorded in Table I. However, the ESC's presence would explain if the measured i_0 was slightly higher than the manufacturer's data; it does not explain a measured value 50% lower. In any case, the difference between the measured and provided values of i_0 does not impact the model since the value of i_0 has very small effect on the torque-speed relation.

B. *Motor Model & Experimental Results*

Figures 4 and 5 compare the theoretical BLDC models to the experimental results. The downward slopes represent the BLDC's torque-speed relationship at PWM duty cycles of both 50% and 100%. The comparison between the theoretical and experimental models is done at $\beta = 100\%$ as well as $\beta = 50\%$ since in many cases, the motor-propeller combinations could not be run at $\beta = 100\%$ without drawing current levels above the motor's limit. This is apparent in Figure 5 where there are too few points at $\beta = 100\%$ to perform a reliable linear regression. In Figure 4, the experimental results allowed for both regressions to be made and the fact that both slopes are parallel is concurrent with the theoretical predictions.

For the experimental data, the PWM duty cycle, β, was assumed to be equal to the percentage of the ESC's signal, ϵ. This is because it is not obvious how to determine the experimental value of β at a particular set of operating conditions. It would be incorrect to assume that β is the ratio of instantaneous speed to the maximum speed obtained with that particular propeller because β and n are directly proportional only if τ is constant. To truly determine if $\beta = \epsilon$, tests would need to run under constant load to see if ϵ and n are directly proportional.

Referring to Figures 4 and 5, it is also apparent that the motor model is not accurate: in both figures the theoretical models' speed-axis intercept is too low and the torque-axis intercept is too high. Working with the model to try and identify the source of error revealed the following conclusions:

- Increasing $v = \beta V_s$ increases both the speed-axis and torque-axis intercepts.
- Increasing K_v increases the speed-axis intercept.
- Increasing R_m decreases the torque-axis intercept.
- Changing i_0 has an insignificant effect on the speed-torque relation.
- Introducing a conversion efficiency factor $\eta < 1$ such that $K_t = \eta \frac{60}{2\pi K_v}$, decreases the torque-axis intercept.

A lower torque-axis intercept is easily obtained by introducing a conversion efficiency factor. On the other hand, doing so also reduces the slope of the $\beta_T = 100\%$ line so much that the experimental results would exceed it. Since this is not possible, lowering the torque-axis intercept alone is not sufficient: the speed-axis intercept would need to be increased as well, but this is difficult to justify. It is possible that the value of K_v used to generate the theoretical model is too low and that this leads to the lower speed-axis intercept. However, this seems unlikely since the value of K_v being used is already 20% higher than the manufacturer's data.

C. *Propeller Model & Experimental Results*

Figures 7 - 14 compare the theoretical propeller models, shown in dashed lines, to the experimental results. Note that the predictions of static thrust in Figure 14 have been increased by 150% to account for the presence of a third blade.

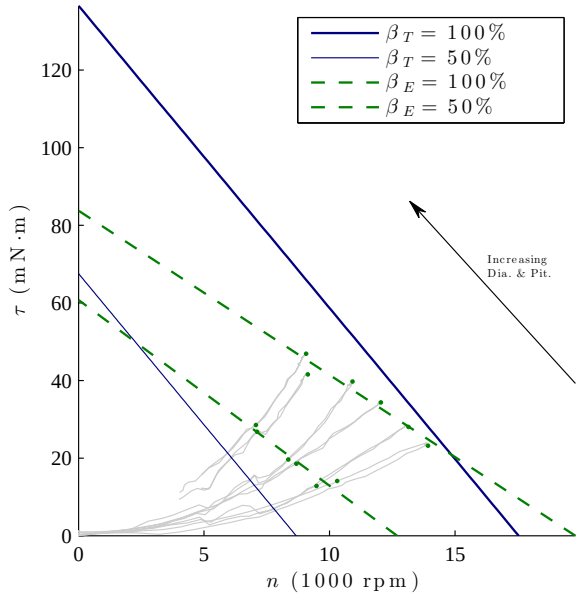

Figure 4. Theoretical and Experimental E-flite Park 300 Motor Performance

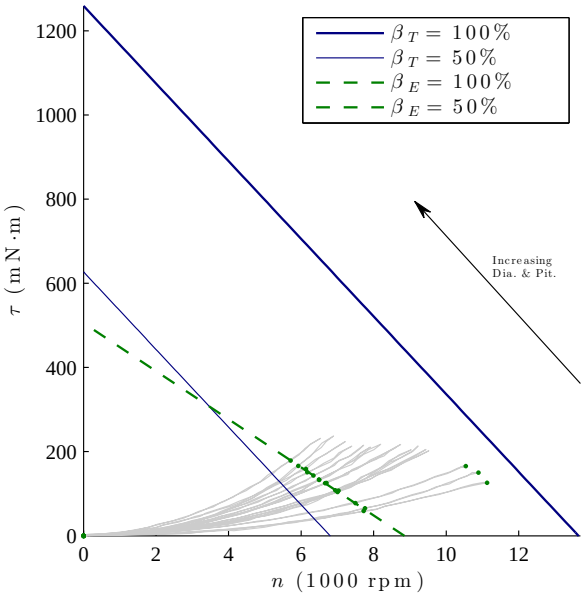

Figure 5. Theoretical and Experimental E-flite Park 480 Motor Performance

Studying the figures, it becomes apparent that:

- A higher diameter or a higher pitch increases thrust.
- Changes in the diameter or pitch have a more significant impact on thrust when the propeller has a smaller diameter

or pitch.

- The model consistently overestimates the experimental results.
- The model more accurately predicts the thrust for smaller propellers. Although the values may not be exact, the spacing between the curves more closely resembles the experimental results.

There are however a few figures which show unexpected experimental results:

- Figure 10: all the propellers provide the same amount of thrust at low and medium speeds.
- Figures 10 - 12: the propellers with the smallest pitch have the highest thrust output at high speeds.

The unexpected results prompted a second series of tests for all propellers. The second tests showed very high repeatability and demonstrated almost exactly the same thrust-speed relationship for all propellers.

Although the propeller model is fairly accurate, a few changes to Staples' constants can yield better results. For example, the plots in Figures 15 and 16 were produced using the constants $K_1 = 1.7$ and $K_2 = 3.8$. These modified constants were determined by trial and error to exemplify how K_1 and K_2 can affect the model. A more rigorous approach would be to write a program which would iteratively try different values and calculate the average error on all propellers in order to select the constants which minimize the error. In addition to changing K_1 and K_2, a third constant K_3 could be introduced to account for variations of C_T as a function of rotational speed. This would be consistent with the findings in two studies at the University of Illinois at Urban-Champaign (UIUC) which measured, amongst other things, the coefficients of thrust for a large number of propellers both statically and dynamically [13]. The modified coefficient of thrust would then take a form such as:

$$C_T = \left(\frac{60}{2\pi}\right)^2 \frac{0.0254^4}{4 \cdot 60^2} K_1^{-K_2} \left(\frac{d}{p}\right)^{K_2-2} n^{K_3} \qquad (14)$$

It is important to keep sample size in mind. For example, the modified coefficients of thrust used in Figures 15 and 16 may be better suited to this particular manufacturer or range of propeller sizes while Staples' coefficients may be more generalized.

D. *Efficiency Mapping*

Having measured the thrust, torque, speed, voltage, and current in various tests, it is possible to calculate the efficiency of the hardware arrangements. In particular, it is possible to calculate the efficiency of the motor independently of the efficiency of the propellers as well as calculate the efficiency of the motor and propeller combination.

The efficiency maps are shown in Figures 17 to 21. The maps are created by 5th order polynomial interpolation over the data points collected in the motor-propeller tests. The electric power is calculated as the product of instantaneous voltage and current while the mechanical power as the product of instantaneous torque and angular speed. The motor, propeller, and combined efficiency maps respectively show interpolated surfaces for the ratio of mechanical to electrical power ($\%W_M/W_E$), the ratio of thrust to mechanical power (gf/W_M), and the ratio of thrust to electrical power (gf/W_E).

These maps could aid in the selection of hardware if one or both of the operating conditions (n, τ) are predetermined. Maximizing efficiency is then a question of choosing a motor and/or propeller such that the efficiency is maximized for the imposed speed/torque.

V. Discussion

The experimental results illustrate that the motor characteristics provided by the manufacturer did not correlate well with the values measured in the laboratory. The data provided by E-flite had an average error of roughly 16% with respect to K_v, an average error of roughly 10% with respect to R_m, and an average error of roughly 50% with respect to i_0. Given the accuracy of the motor model, the errors in the measurement of K_v and R_m are sufficiently small to warrant using the manufacturer's data to construct the theoretical model, especially since i_0 has an insignificant influence on the model's torque-speed relationship.

Secondly, the results show that the motor model does not accurately reflect the motor's no-load speed, possibly because of an underestimated value for K_v. The results also show that the model does not accurately reflect the motor's stall-torque, though here the model could be amended by adjusting the estimated value of K_t by means of an conversion efficiency factor so that $K_t = \eta \frac{60}{2\pi K_v}$.

Thirdly, the results show that the propeller model is fairly accurate and constitutes an interesting alternative to conventional propeller thrust estimations. Although the model uses propeller diameter and pitch as the only geometric inputs, Staples' relation estimates the thrust output reasonably well, particularly for small propellers. In the future, it would be interesting to acquire test data from a larger number of propellers in order to review Staples' constants and possibly improve the model by adding a speed dependency to the generalized thrust coefficient. Furthermore, it would be interesting to investigate if a similar relation could be developed for the propeller's torque coefficient. If both the thrust and torque could be estimated as a function of speed, then it would make it possible to couple the theoretical motor and propeller models by using the propeller model's outputs as inputs to the motor model as shown in Figure 6.

VI. Conclusion

This paper aimed to validate simple motor and propeller models with the purpose of selecting an appropriate motor-

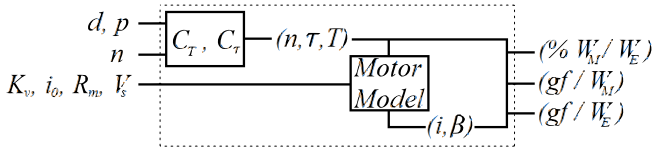

Figure 6. Inputs and Outputs to the Coupled Thrust-Torque Models

propeller combination. It was possible to independently validate the motor and propeller models by decoupling them and studying the results separately.

REFERENCES

[1] S. Recoskie, A. Fahim, W. Gueaieb, and E. Lanteigne, "Experimental testing of a hybrid power plant for a dirigible uav," Journal of Intelligent & Robotic Systems, vol. 69 (1-4), 2013, pp. 69–81.

[2] P. Pounds, R. Mahony, and P. Corke, "Modelling and control of a large quadrotor robot," Control Engineering Practice, vol. 18 (7), 2010, pp. 691–699.

[3] November 2013.

[4] P. Pounds, R. Mahony, J. Gresham, P. Corke, and J. M. Roberts, "Towards dynamically-favourable quad-rotor aerial robots," in Proceedings of the 2004 Australasian Conference on Robotics & Automation, Australian Robotics & Automation Association, 2004.

[5] P. Lindahl, E. Moog, and S. R. Shaw, "Simulation, design, and validation of an uav sofc propulsion system," Aerospace and Electronic Systems, IEEE Transactions on, vol. 48 (3), 2012, pp. 2582–2593.

[6] W. Khan and M. Nahon, "Toward an accurate physics-based uav thruster model," Mechatronics, IEEE/ASME Transactions on, vol. 18 (4), 2013, pp. 1269–1279.

[7] Honeywell, How to select Hall-effect sensors for brushless dc motors, 2015.

[8] K. Sitapati and R. Krishnan, "Performance comparisons of radial and axial field, permanent-magnet, brushless machines," Industry Applications, IEEE Transactions on, vol. 37 (5), Sep 2001, pp. 1219–1226.

[9] A. Cavagnino, M. Lazzari, F. Profumo, and A. Tenconi, "A comparison between the axial flux and the radial flux structures for pm synchronous motors," Industry Applications, IEEE Transactions on, vol. 38 (6), Nov 2002, pp. 1517–1524.

[10] S. Recoskie, Autonomous Hybrid Powered Long Range Airship for Surveillance and Guidance, Ph.D. thesis, University of Ottawa, 2014.

[11] A. Imam and R. Bicker, "Design and construction of a small-scale rotorcraft uav system," International Journal of Engineering Science and Innovative Technology (IJESIT), vol. 2, 2014.

[12] J. R. Hendershot and T. J. E. Miller, Design of brushless permanent-magnet machines, Motor Design Books, 2010.

[13] G. K. A. John B. Brandt, Robert W. Deters and M. S. Selig, "Uiuc propeller database," Tech. rep., University of Illinois at Urban-Champaign, 2015.

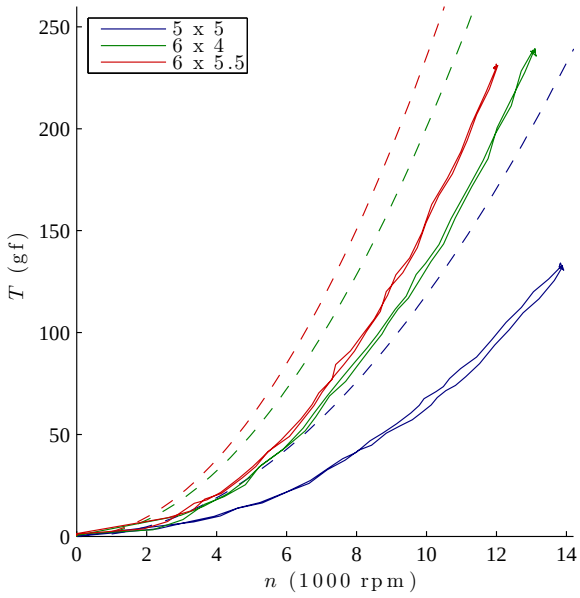

Figure 7. Theoretical and Experimental 5" and 6" Propeller Performance

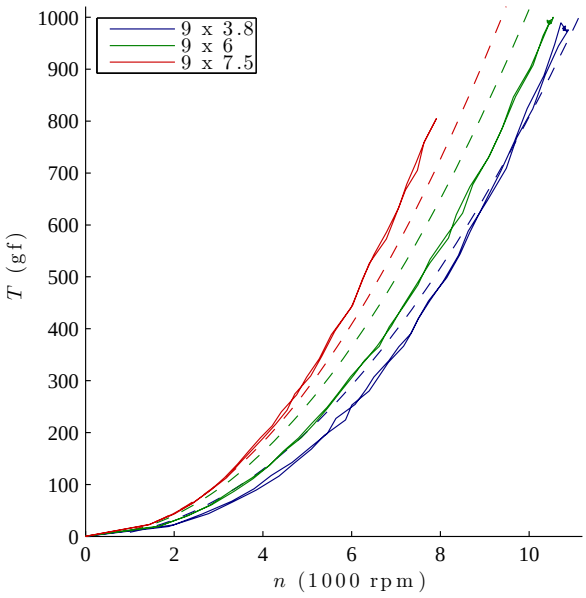

Figure 9. Theoretical and Experimental 9" Propeller Performance

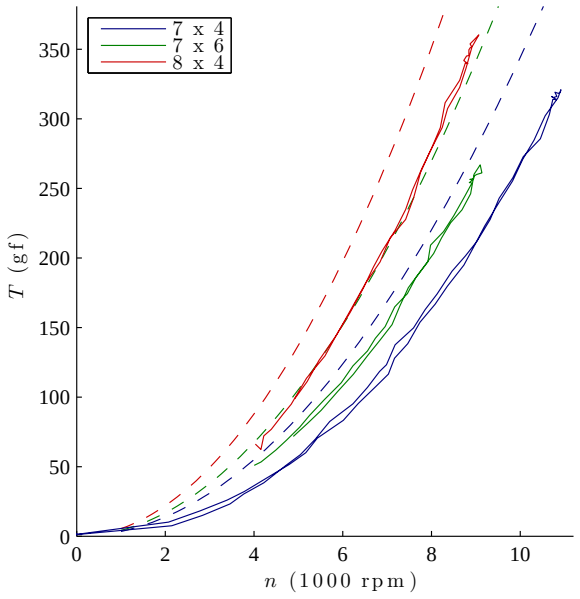

Figure 8. Theoretical and Experimental 7" and 8" Propeller Performance

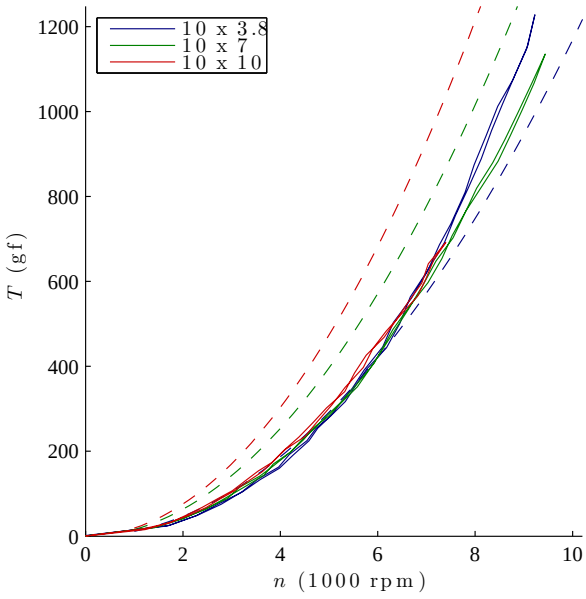

Figure 10. Theoretical and Experimental 10" Propeller Performance

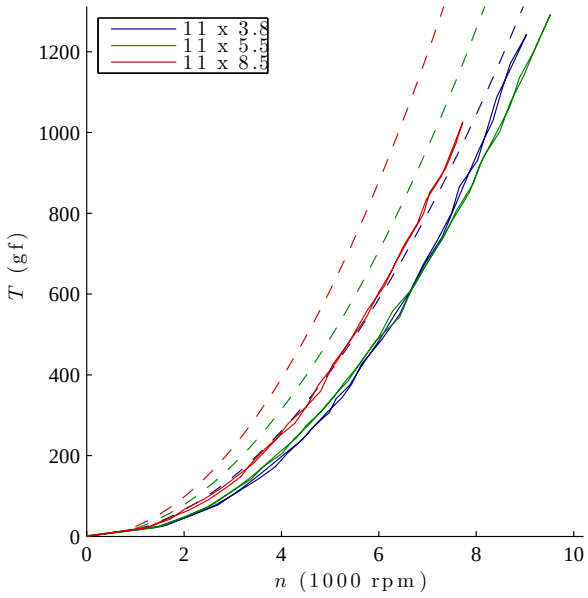

Figure 11. Theoretical and Experimental 11” Propeller Performance

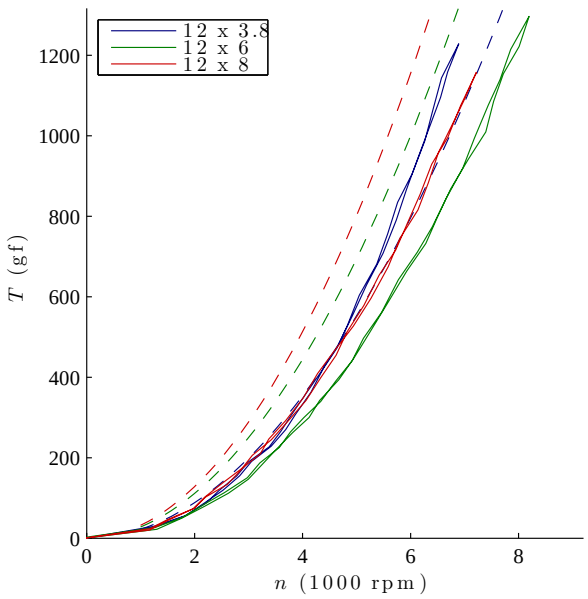

Figure 12. Theoretical and Experimental 12” Propeller Performance

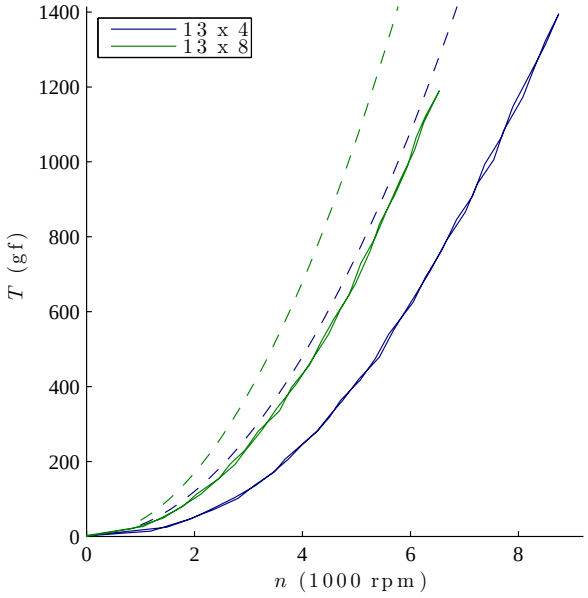

Figure 13. Theoretical and Experimental 13” Propeller Performance

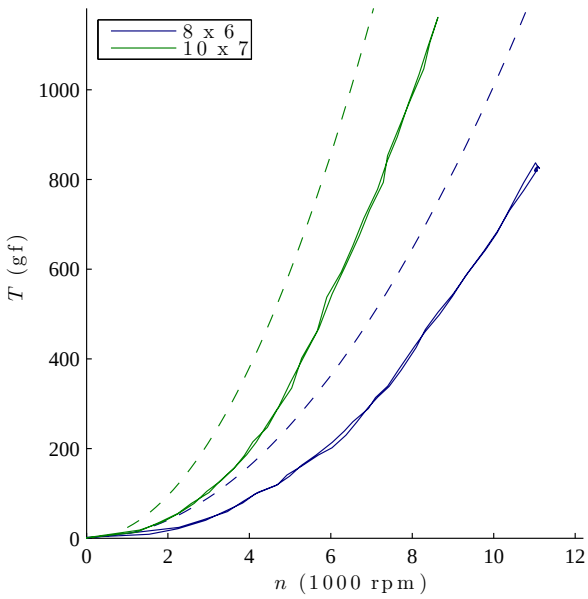

Figure 14. Theoretical and Experimental Three-blade Propeller Performance

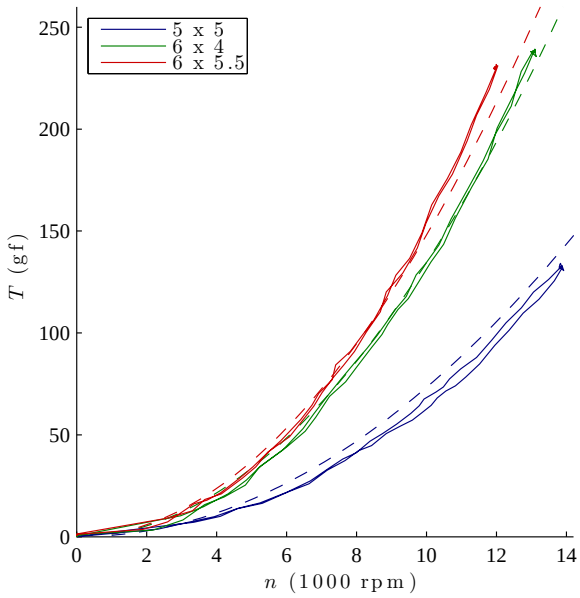

Figure 15. Modified Theoretical and Experimental 5" and 6" Propeller Performance

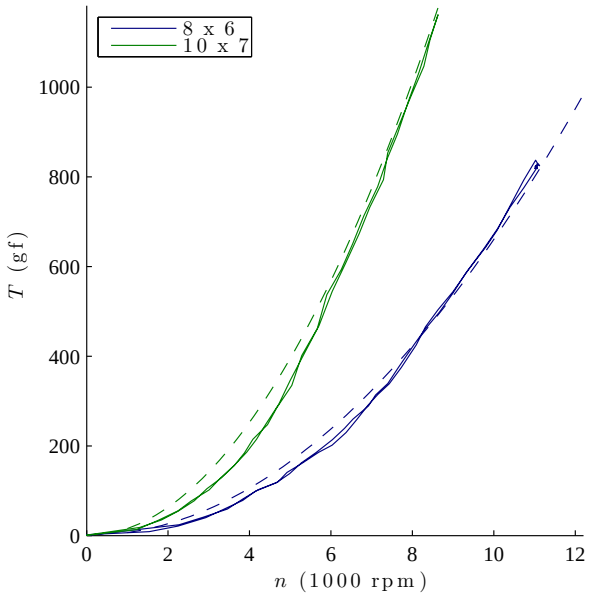

Figure 16. Modified Theoretical and Experimental Three-blade Propeller Performance

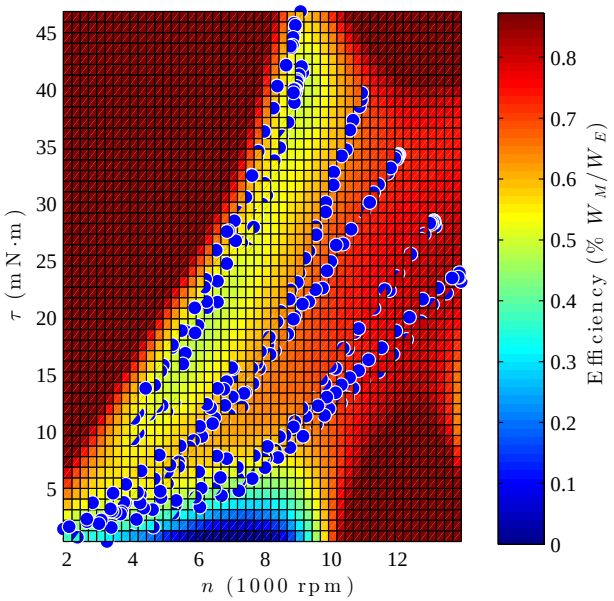

Figure 17. E-flite Park 300 Motor Efficiency Map

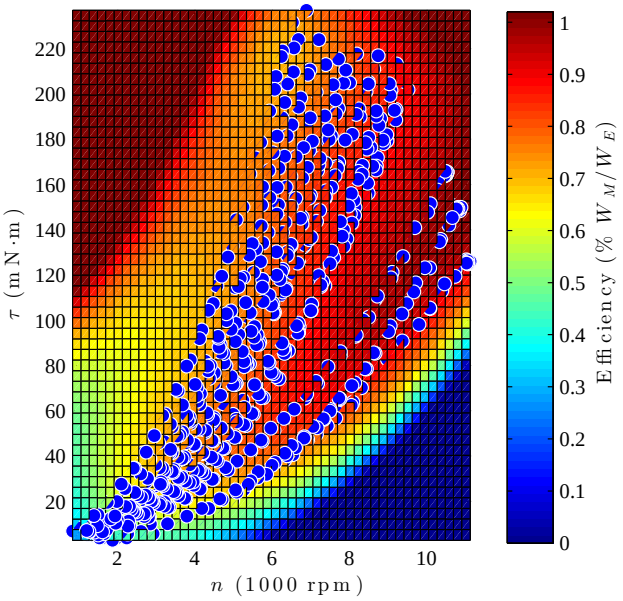

Figure 18. E-flite Park 480 Motor Efficiency Map

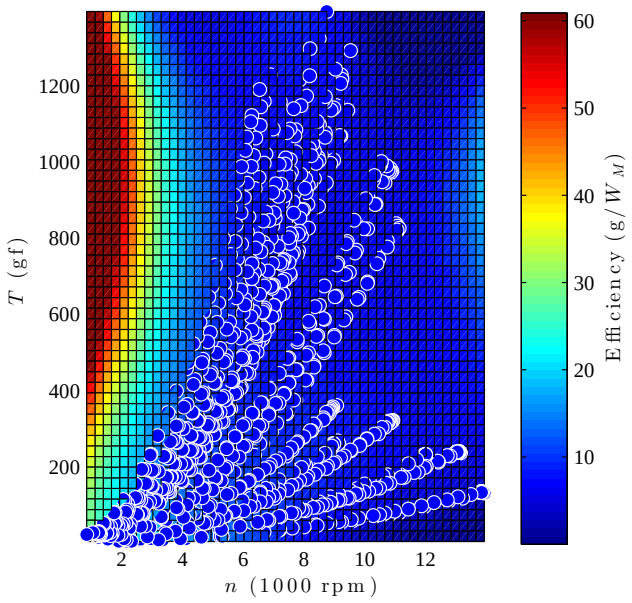

Figure 19. Propeller Efficiency Map

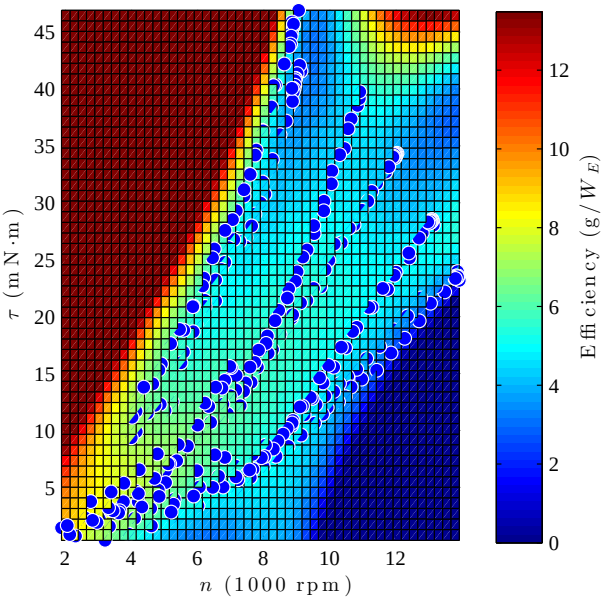

Figure 20. E-flite Park 300 Motor-Propeller Efficiency Map

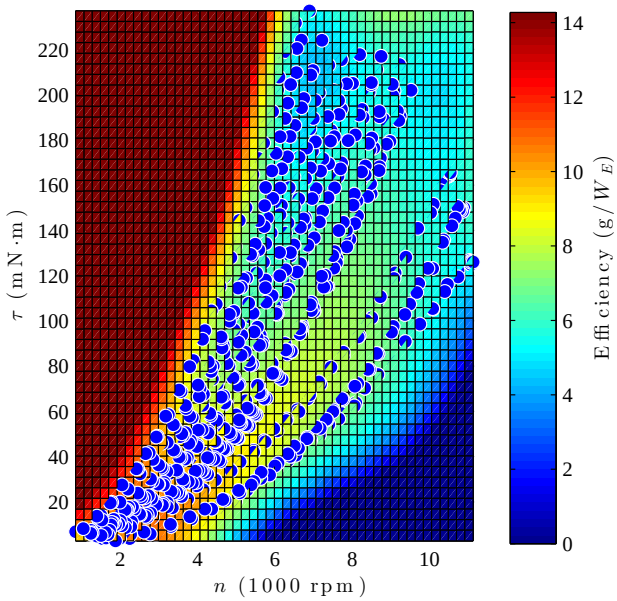

Figure 21. E-flite Park 480 Motor-Propeller Efficiency Map